Nowcasting severe convective activity over southeast India using ground-based microwave radiometer observations

A. Madhulatha,[1] M. Rajeevan,[2] M. Venkat Ratnam,[1] Jyoti Bhate,[1] and C. V. Naidu[3]

[1] In the present study, the feasibility of nowcasting convective activity is examined by using thermodynamic indices derived from the ground-based microwave radiometer (MWR) observations located at a tropical station, Gadanki (13.5°N, 79.2°E). There is a good comparison between thermodynamic parameters derived from MWR and colocated GPS radiosonde observations, indicating that MWR observations can be used to develop techniques for nowcasting severe convective activity. Using MWR observations, a nowcasting technique was developed with the data of 26 thunderstorm cases observed at Gadanki. The analysis showed that there are sharp changes in some thermodynamic indices, such as the K index, the humidity index, precipitable water content, the stability index, and equivalent potential temperature lapse rates, about 2–4 h before the occurrence of thunderstorm. A superepoch analysis was made to examine the composite temporal variations of the thermodynamic indices associated with the occurrence of thunderstorms. The superepoch analysis revealed that 2–4 h prior to the storm occurrence, appreciable variations in many parameters are observed, suggesting thermodynamic evolution of the boundary layer convective instability. It is further demonstrated that by monitoring these variations it is possible to predict the ensuing thunderstorm activity over the region at least 2 h in advance. The association between the temporal evolution of thermodynamic indices and convective activity has been tested for the independent case of nine thunderstorms. The present results suggest that ground-based MWR observations can be used effectively to predict the occurrence of thunderstorms at least 2 h in advance.

1. Introduction

[2] Thunderstorms are mesoscale convective systems which cause devastating consequences like lightning, heavy precipitation, hail, and wind gusts. These weather systems can disrupt public life, satellite launch operations, air transport and bring out human and economic losses. In general, the time span of these convective systems is about 20–30 min, which makes it difficult to forecast these weather features in advance. Prediction of such systems using weather prediction models is still difficult because of relative coarse resolution, lack of observations of the initial state, and the limited predictability of small mesoscale phenomena [*Rajeevan et al.*, 2010]. Attempts to predict these events using weather prediction models encounter problems from imperfect knowledge of the state of the atmosphere on the mesoscale, in particular regarding the three main ingredients which invoke thunderstorms, i.e., moisture availability, convective instability and lifting mechanism [*Kober and Tafferner*, 2009].

[3] Deep convection requires the presence of a conditionally unstable lapse rate, so that parcels lifted adiabatically from the planetary boundary layer (PBL) become more buoyant than their environment. The latent heat release by condensation provides the thermal energy required to give positive buoyancy to provide vertical momentum sufficient to carry parcels from the PBL to the level of free convection [*Colby*, 1984]. Previous studies [*Beebe*, 1958; *Carlson et al.*, 1983; *Colby*, 1984; *Sanders*, 1986; *Sanders and Blanchard*, 1993] on the pre convective environment highlight the importance of changing PBL heat and moisture for the initiation of deep convection. Increasing heat and moisture reduces the level of free convection and increase parcel's convective available potential energy (CAPE) [*Bluestien and Parker*, 1993]. In addition, the presence of convective inhibition energy (CINE, in the form of capping inversion) may prevent the realization of this potential energy within the free troposphere [*Sanders and Blanchard*, 1993]. The knowledge of balance between PBL equivalent potential temperature and the intensity of the capping inversion monitored at high time resolution is critical to a successful nowcast of thunderstorm occurrence [*Feltz and Mecikalski*, 2002].

[1]National Atmospheric Research Laboratory, Gadanki, India.
[2]Ministry of Earth Sciences, New Delhi, India.
[3]Department of Meteorology and Oceanography, Andhra University, Visakhapatnam, India.

Corresponding author: A. Madhulatha, National Atmospheric Research Laboratory, Gadanki P.O., Chittoor District, Andhra Pradesh 517 112, India. (madhulatha@narl.gov.in)

[4] Very short period forecasting of the future location of convective storms has historically been based on extrapolation of radar reflectivity echoes. The accuracy of these forecasts generally decreases very rapidly during the first 30 min because of the very short life time of individual convective storms. For forecasts periods beyond ~20 min, techniques for forecasting the initiation, growth, and dissipation of convective storms are essential [*Browning*, 1980; *Wilson and Mueller*, 1993; *Wilson et al.*, 1998; *Hering et al.*, 2004]. Storm location and intensity are primarily determined by mesoscale stability, wind fields and in particular convergence lines. Methods under development for forecasting storm evolution are knowledge-based expert systems, statistical techniques and explicit numerical forecast models that are initialized with radar data. The accurate forecasts of convection initiation will require initial conditions for the dynamical, thermodynamical, and microphysical fields, which in some cases are beyond our present observing capabilities. In other words, skillful numerical storm prediction require that NWP models are run over large enough domains to capture the large-scale forcing and high enough resolution that the storm structure can be initialized from radar data. The knowledge-based expert system utilizes radar, satellite, boundary layer profilers, lightning network, high-density surface observations, and upper air weather observations (soundings). These systems may also make use of numerical model output and utilize fuzzy logic techniques and neural networks [*Wilson et al.*, 1998]. During the recent years, a variety of statistical techniques have been used to develop forecast models for thunderstorms and lightning [*Reap*, 1994; *Lambert et al.*, 2005; *Shafer and Fuelberg*, 2006]. In a recent study by *Rajeevan et al.* [2012], a statistical model based on binary logistic regression was developed for predicting probability of lightning occurrence over southeast India using the perfect prognostic method (PPM). For real time forecasts, predictors are derived from 12 h predictions using the WRF model. The model showed some encouraging results in predicting the probability of lightning over the region about 3–12 h in advance.

[5] As discussed earlier, the other method of nowcasting is to examine stability/convective indices derived mainly from the upper air soundings to explain the thermodynamic evolution of the boundary layer convective instability [*Feltz et al.*, 2003]. In operational weather forecasting, it is common to examine the temperature and humidity profiles measured by radiosondes and the derived instability indices in nowcasting heavy rain and thunderstorms [*McCann*, 1994; *Geerts*, 2001; *Manzato*, 2003; *Lee*, 2007]. There are many previous studies [*Tuduri and Ramis*, 1997; *Manzato*, 2003; *Marinaki et al.*, 2006] of correlating convective activity with the radiosonde derived instability indices. However, ordinary upper air observations by radiosonde are taken only twice a day, which are not sufficient to monitor atmospheric structures vertically for a short-term forecast. This is because precipitation systems develop rapidly and thermodynamic properties of troposphere could change rapidly [*Güldner and Spänkuch*, 1999]. Therefore, more frequently available thermodynamic information is of great benefit for severe weather nowcasting. This problem can be solved to large extent with ground-based microwave radiometer, which gives continuous profiles of temperature and humidity with high temporal resolution.

[6] Over the last 25 years, ground-based remote profiling of various atmospheric parameters has found increasing applications in atmospheric studies where its high vertical and temporal resolution and extended vertical coverage are giving scientists a clearer understanding of atmospheric processes in the troposphere. Various studies have been carried out to observe continuously the atmosphere in the boundary layers for short-term weather forecasting, using various remote sensing instruments, such as a wind profiler, radar, lidar, and microwave radiometers [*Clifford et al.*, 1994; *Wilczak et al.*, 1996; *Güldner and Spänkuch*, 2001; *Won*, 2009]. *Ware et al.* [2003] compared radiometric, radiosonde and forecast soundings for evaluating the accuracy of radiometric temperature and water vapor soundings. Studies by *Koffi* [2007] have shown that the fine temporal resolution of convective indices may be valuable for thunderstorm nowcasting as well as for basic studies on convection evolution.

[7] Microwave radiometer (MWR) has the advantage of continuous monitoring of atmosphere up to 10 km to cover the temporal and spatial gaps of synoptic networks by radiosonde measurements. Ground-based MWRs [*Rose and Czekala*, 2003; *Knupp et al.*, 2009] retrieve the temperature and humidity profiles up to 10 km by measuring the radiation intensity at a number of frequency channels in the microwave spectrum that are dominated by atmospheric water vapor, cloud liquid water and molecular oxygen emissions. A comprehensive study by *Chan*, [2009] during a field experiment discussed the importance of the MWR profiles in nowcasting of intense convective weather over Hong Kong. Later, *Chan and Hon* [2011] elaborately described the importance of the MWR derived indices, and their usage in nowcasting by correlating the derived variables with the lightning activity. The high temporal resolution monitoring of rapid atmospheric destabilization is especially important for nowcasting severe convection [*Feltz et al.*, 2003]. The determination of water vapor mixing ratio and temperature profiles within the troposphere using microwave radiometer enables high temporal monitoring of stability indices. These data sets provide a unique, real time assessment of the preconvective atmosphere, not available from conventional sounding observations usually made twice daily.

[8] Recently, a ground-based MWR was installed at the National Atmospheric Research Laboratory (NARL), at Gadanki (13.5°N, 79.2°E), a semiarid station located over Southeast India. The continuous measurements of temperature and humidity profiles up to 10 km with high temporal resolution (~5 min) obtained from MWR can be used to derive thermodynamic stability indices, which will give an indication of the degree of convective instability of the troposphere. In the present study, we explore the possibility of nowcasting thunderstorm activity over the southeast Indian region using the ground-based MWR and other observational systems. For identifying the genesis of thunderstorm activity, lightning data recorded by the Electric Field mill available at the observational site were also considered. Electric field intensity greater than 2000 V/m is identified as thunderstorm activity. Altogether, 25 thermodynamic indices were considered, including the single-level indices depending on temperature and dew point at specific levels, such as the K index (KI), the humidity index (HI), total total index (TTI), integrated parameters like convective available potential energy (CAPE), moisture parameters like

precipitable water content, relative humidity, layer thickness, stability index, lapse rate at different levels based on equivalent potential temperature, and the shape factor (SF) [*Walker et al.*, 2008]. The estimation of all these indices is described in Appendix A.

[9] The present paper reports the application of multi-wavelength, ground-based MWR observations at Gadanki in nowcasting thunderstorms over the region. The equipment setup of MWR and methodology is described in section 2. Validation of MWR data with GPS radiosonde and the performance of MWR during severe convection are examined by correlating the MWR derived stability indices with radiosonde derived stability indices are discussed in section 3. To obtain the composite picture of stability indices during the thunderstorm events, a superepoch analysis has been carried out to examine the temporal variations in various stability indices prior to the storm occurrence. These results are discussed in section 4. The inference established from superepoch analysis is tested for an independent verification of nine thunderstorm cases is discussed in section 5. Conclusions are drawn in section 6.

2. Data and Methodology

[10] In the present study, MWR and GPS radiosonde observed temperature and humidity profiles during the period, June to December 2011 were used. MWR used in the present study is a MP-3000A temperature, humidity and liquid profiler (manufactured by Radiometrics Corporation), which operates in 21 K band (22–30 GHz) and 14 V band (51–184 GHz) microwave channels. It measures the radiation intensity of the sky in 35 different frequency channels both in oxygen and water vapor bands, which are primary absorbers of the atmospheric radiation in the atmosphere. Neural network retrieval method has been constructed to retrieve the temperature profiles from the brightness temperature measurements [*Chan and Lee*, 2011]. Retrieval of temperature and humidity profiles from the radiation intensity measurements of the radiometer is accomplished by neural network methods based on historical radiosonde data, using a radiative transfer model to simulate the observations of a radiometer [*Chan*, 2009]. In this study neural network algorithm was trained by using high-resolution radiosonde data from the same location for the period 2006 to 2009. MWR scans the atmosphere in zenith and off zenith directions in different elevations at fixed angles. For the present study, the temperature and humidity profiles in the zenith direction only are only taken, which are normally available in every 4–5 min interval up to 10 km altitude. The vertical soundings of temperature and humidity obtained from the Meisei radiosonde balloon ascents launched at around 1200 UTC (1730 local time (LT)) daily from Gadanki are also taken. The accuracy of temperature and relative humidity sensors of radiometer provided by radiometrics are 0.5 K and 2%, respectively which are at par with radiosonde observations [*Nath et al.*, 2009].

[11] In addition to this, electric field mill (EFM) measurements are also used to identify thunderstorm activity. EFM is a real-time lightning system which monitors the development and dissipation of overhead lightning threats by measuring local atmospheric electric field. EFM measures the electric field intensity in the local area. There is always vertical electric field in the atmosphere. In fair weather this

electric field is around 0 to 200 V/m. In stormy weather it is much higher because of presence of electric charges on thunder clouds. By the time the electric field reaches 2000 V/m the probability of lightning is significant. EFM theory is based on basic laws of electromagnetism. When a conducting plate is exposed to electric field, a charge will be induced proportional to electric field and the plate area. EFM creates an alternating electric field using a motor driven rotor and stator arrangement, which is easier to measure. In addition to detecting the electric field changes associated with thunderstorms, EFMs also detect variety of other signals not associated with thunderstorms like blowing sand or dust, blowing snow, charge separation in nonlightning producing showers, charge separated when raindrops splash on or near the instrument. This wide variety of signals can lead to false alarms when EFMs are used for lightning warnings, but the amount of such false alarms will depend on the field threshold used for identifying thunderstorm activity as well as frequency, duration and intensity of such events [*Murphy et al.*, 2008].

3. Results and Discussions

3.1. Validation of MWR Data With GPS Radiosonde Data

[12] The temperature and humidity profiles derived from MWR for the period June to December 2011 are compared with the profile derived from GPS radiosonde observations, from the same location. The mean profiles for temperature and vapor density and difference between temperature and vapor density along with standard deviations derived from MWR and GPS radiosonde for the period June through December 2011 are shown in Figure 1. A very close agreement in temperature profiles between MWR and GPS radiosonde are found (shown in Figure 1a). The comparision for
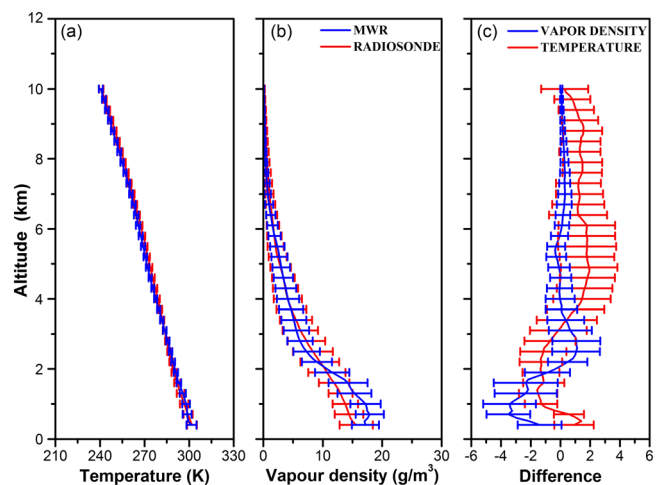
Figure 1. Composite profiles of (a) temperature and (b) vapor density along with standard deviation observed with GPS radiosonde (red solid line) and MWR (blue solid line) during June through December 2011. (c) Difference between GPS radiosonde and MWR temperature (red solid line) and vapor density (blue solid line) along with standard deviation of errors.

vapor density profiles (Figure 1b) are better in middle to upper troposphere and at the lower levels (below 3 km), MWR observations show a wet bias compared to the radiosonde observations in the lower levels. However, these results on dry bias of radiosonde are consistent with the earlier observations by *Westwater et al.* [2003] and *Cady-Pereria et al.* [2008]. Difference between GPS radiosonde and MWR for temperature and vapor density profiles along with standard deviation are shown in Figure 1c. Temperature of MWR in the lower levels and above 4 km, shows cold bias with the magnitude of 1°C and vapor density of MWR shows wet bias below 2 km and dry bias up to 4 km when compared with radiosonde measurements (shown in Figure 1c). For vapor density, wet bias of MWR at lower levels and dry bias higher up are coinciding with the results of [*Chan*, 2009]. Since the measurement principles of the two instruments are different (Volume integral above a fixed location on the ground for Radiometers vs. point measurement of a drifting balloon for radiosonde), there are biases and spreads of the data points, but the two data sets are following the similar trends in the evolution of the temperature and humidity inside the troposphere *Chan and Hon* [2011].

3.2. Correlation of Thermal Indices Derived From MWR and GPS Radiosonde Data

[13] In this section, we examine the correlations of thermodynamic indices derived from the MWR and GPS radiosonde observations. Since the radiosonde data are available only at 1200 UTC, we used the MWR data of the corresponding hour for the analysis. Using the temperature and relative humidity profiles obtained from GPS radiosonde and MWR, 25 thermodynamic (including moisture variables) parameters are computed (details of the 25 indices are given in Appendix A). The correlation coefficients of calculated 25 thermodynamic indices are shown in Table 1.

Table 1. Correlation Values Between GPS and MWR for Different Thermodynamical Parameters

Parameter	R
LI	0.18
KI	0.91
TTI	0.58
HI	0.95
LCAPE2	0.32
CINE	0.15
CONVTEMP	0.50
SF	0.37
PW	0.98
MEANRH$_{950-850hPa}$	0.88
RHFRZL	0.84
MEANLAYRH	0.98
THICKNESS$_{950-850hPa}$	0.60
THICKNESS$_{850-500hPa}$	0.27
THICKNESS$_{700-400hPa}$	0.14
THICKNESS$_{500-300hPa}$	0.34
$(\theta_{es}-\theta_e)_{950hPa}$	0.92
$(\theta_{es}-\theta_e)_{850hPa}$	0.75
$(\theta_{es}-\theta_e)_{500hPa}$	0.79
LR$_{950-700hPa}$	0.75
LR$_{700-400hPa}$	-0.07
LR$_{400-300hPa}$	0.04
θ_e LR$_{950-700\ hPa}$	0.57
θ_e LR$_{700-400\ hPa}$	0.76
θ_e LR$_{400-300\ hPa}$	0.30

All parameters are well correlated each other except the following four parameters, LI, CINE, Thickness (700–400 hPa) and LR (700–400 hPa). The scatterplots of 15 thermodynamic indices (having a correlation >0.5) derived from the MWR and radiosonde data are shown in Figures 2 and 3. In general, the MWR derived indices and radiosonde derived indices are well correlated. Among all the indices, single-level indices like KI, TTI, HI and moisture parameters like PW, MEANLAYRH, and stability index $(\theta_{es} - \theta_e)_{950hPa}$ show very high correlation of 0.9 which is significant at the 99% confidence level. Among all the moisture indices, PW showed the best correlation of 0.98. Fairly good correlation of the parameters KI, HI, TTI are persistent with previous observations by [*Chan and Hon*, 2011]. The correlation analysis suggests that the quality of MWR profiles is adequate enough to calculate the stability indices using MWR data which can explain thermodynamic structure of the troposphere. Therefore, for further analysis, we have used MWR data to develop methods for nowcasting convective activity over the region.

3.3. Relationship Between the Genesis of Thunderstorm Activity and Thermodynamical Indices

[14] The variation of MWR derived thermodynamic indices and the occurrence of thunderstorm activity is examined in this section. By using a single index, namely, KI, *Chan* [2009] demonstrated a good correlation between lightning activity and the instability index, KI. In this section, an attempt has been made to identify precursors of thunderstorm genesis by examining the variations of MWR derived thermodynamic indices and the occurrence of thunderstorm. A thunderstorm event is defined as the event in which the associated observed electric field strength (measured by EFM) is greater than 2000 V/m.

[15] The variations of thermodynamic parameters associated with a thunderstorm event are examined and illustrated by considering a case study of severe thunderstorm occurred over Gadanki. Using the EFM data, a severe thunderstorm observed around 1700 UTC on 27 July 2011 was identified (Figure 4). The temporal variations in basic parameters associated with storm are studied using MWR observations. The continuous temperature and moisture profiles derived from MWR provide unique perspective on the evolution of the thermodynamic structure of convective instability associated with the storm. Sharp increase in water vapor density and fluctuations in temperature are clearly visible during the evolution of the storm. The presence of a deep convective cloud is seen from the large amount of cloud liquid water extending up to 400 hPa. Even though EFM showed changes in the electrical field exceeding 2000 V/M around 1700 UTC only, large-scale convective cloud development was observed from 1300 UTC. It is interesting to note that convective available potential energy (CAPE) increased sharply in the afternoon (almost 6 h in advance); however, it decreased sharply during the occurrence of the storm (Figure 5). This case study illustrated the promise for nowcasting the occurrence of convective activity based on continuous temperature, moisture monitoring and unique cloud liquid soundings in the lower troposphere available from MWR.

[16] To understand the variations of different thermodynamic parameters associated with the thunderstorms, we have examined the 25 parameters tabulated in Table 1.
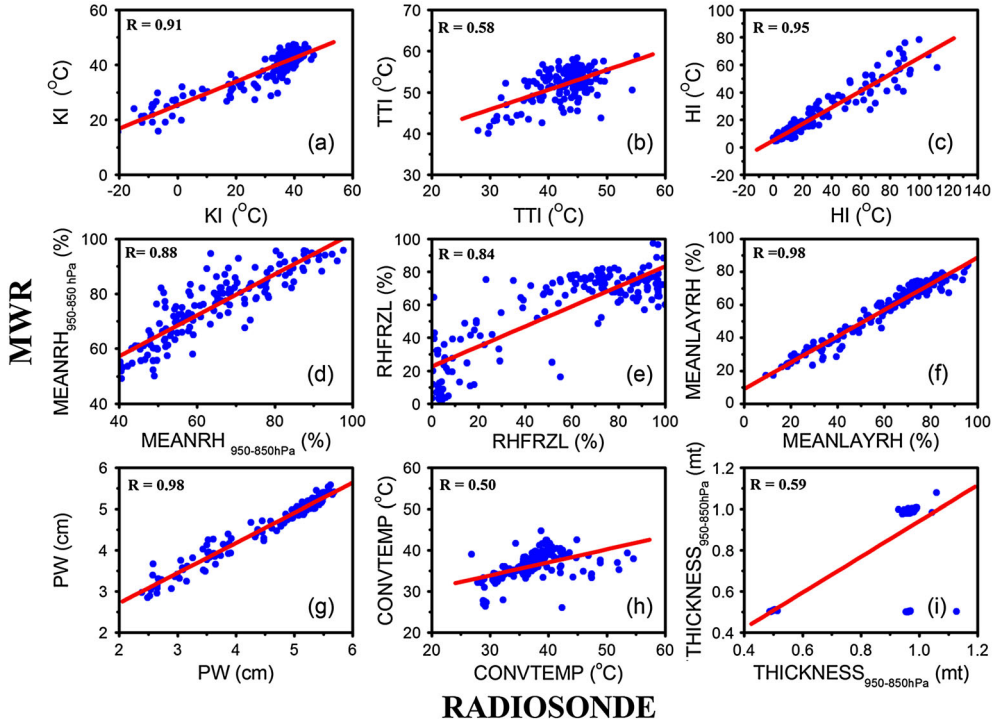
Figure 2. Scatterplots of different thermal and dynamical instability indices derived from GPS radiosonde and MWR. The correlation coefficient values are given in the plot (N = 162).
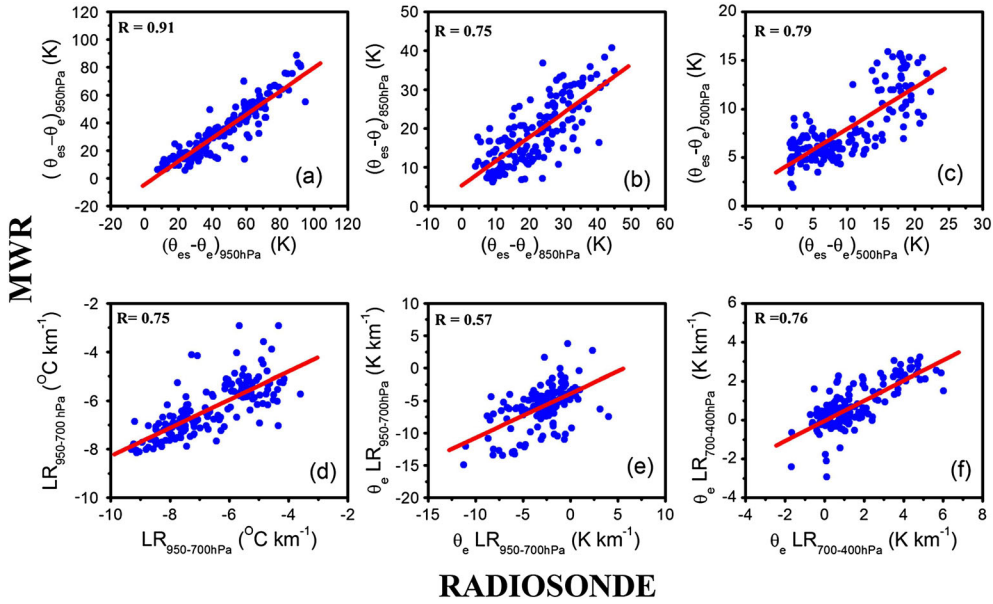
Figure 3. Same as Figure 2, but for the stability index (θ_{es} - θ_e) at different levels, lapse rate at 950–850 hPa, and θ_e lapse rate at different levels.

However, the correlation between MWR and radiosonde observations is more than 0.5 only for 15 parameters (Table 1). Among the 15 parameters, we find eight parameters which consistently showed similar variations associated with the occurrence of thunderstorms. The eight parameters thus identified are, KI, HI, PW, MEANRH$_{950-850hPa}$, (θ_{es}-θ_e)$_{950hPa}$, (θ_{es}-θ_e)$_{500hPa}$, θ_e LR$_{950-700\ hPa}$, θ_e LR$_{700-400\ hPa}$. These parameters explain the variations in temperature, moisture and

stability state of atmosphere which are the basic ingredients for thunderstorm development. A brief description of these eight parameters is as follows.

[17] KI represents the thunderstorm potential as a function of vertical temperature lapse rate, dew point temperature at 850 hPa and the depth of the moist layer at 700 hPa [*George*, 1960]. KI > 30 represents an atmospheric potential for thunderstorms to occur [*Haklander and van Delden*, 2003].
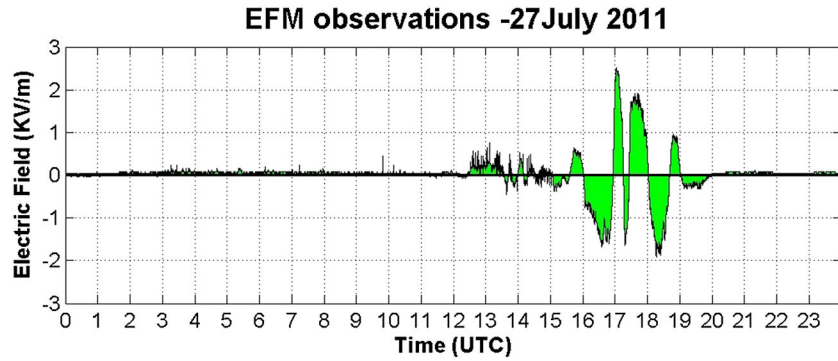
Figure 4. Time series of electrostatic field measured from EFM for the thunderstorm during 27 July 2011.
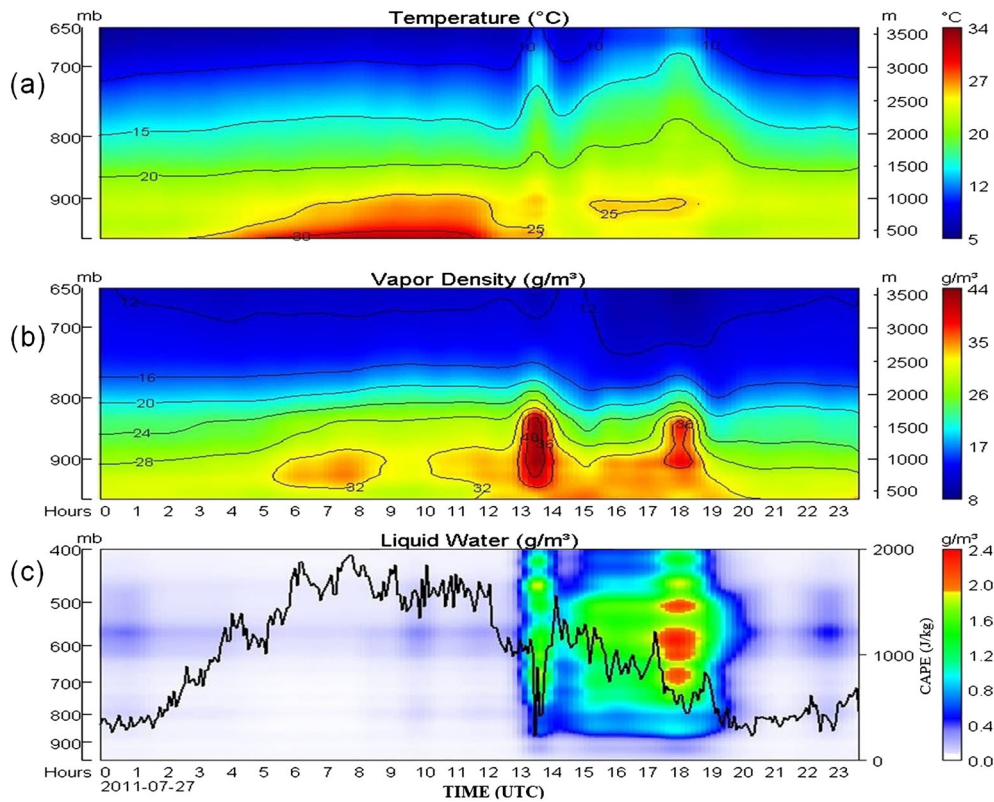
Figure 5. Evolution of atmospheric parameters derived from MWR observations during the genesis of the thunderstorm on 27 July 2011.

Humidity Index HI assesses the degree of saturation at the mandatory levels 850, 700, and 500 hPa [*Jacovides and Yonetani*, 1990]. HI≤30 is suggested as a threshold for thunderstorms, and thunderstorms are more likely for smaller values [*Litynska et al.*, 1976]. It explains the importance of deep layer of high relative humidity in the generation of thunderstorms. A parameter suitable to quantify the amount of water vapor potentially available is precipitable water (PW) [*Dupilka and Reuter*, 2005]. PW is defined as the depth of liquid water which would be present in a column of unit cross section if all the water vapor in that column throughout the depth of atmosphere were condensed. The amount of water vapor available to storm should affect the amount of precipitation generated and as a result the potential for evaporation [*Brooks et al.*, 1994]. High values of

PW in clear air often become antecedent conditions prior to the development of heavy precipitation and flash floods. Relative humidity is a measure of how close air is to saturation at a specific temperature, always expressed as a percentage. Since moisture is important for convective initiation, therefore the amount of relative humidity from surface to boundary layer (MEANRH$_{950-850hPa}$) is very important factor for genesis of storm.

[18] Equivalent potential temperature (θ_e) is a conserved quantity under both dry and moist adiabatic ascent and is a measure of atmospheric stability. The decrease of θ_e with height explains convective or potential instability which accounts the vertical distribution of water vapor. Saturated equivalent potential temperature (θ_{es}) is the value of (θ_e) if air at a given temperature would have if it were saturated.

If θ_{es} of the environment decreases with height then a parcel can become positively buoyant and reach saturation which implies conditional instability. Conditional instability is most appropriate parameter for identifying regions favorable for convection since it is a function of temperature lapse rate only. On a climatological basis both conditional and convective instability exists essentially everywhere in the tropics, so for evaluating favored locations capable for supporting deep convection, both instabilities should be considered [Khalsa, 1989]. The most accurate method of explaining the atmospheric stability is to consider both convective and conditional instabilities.

[19] Stability index (θ_{es}-θ_e) at different levels explains the saturation state of atmosphere. A higher difference implies the atmosphere is unsaturated. The decrease of θ_e with height is θ_e lapse rate (θ_e LR), which explains the stability of atmosphere. Generally, θ_e LR decreasing with height corresponds to unstable atmosphere.

[20] For the present case study of 27 July 2011, we have examined the variations of these eight parameters and the results are shown in Figure 6. Storm initiation time around 1700 UTC is considered as 0 h and variations from -6 to +6 h are shown. The time window shows the thunderstorm episode. From Figures 6a–6d it is clear that before the genesis of storm, the above explained parameters show sharp variations indicating the occurrence of thunderstorm. Relative increase in KI is observed 2-1 h prior to the storm genesis which represents the increase in low-level moisture content, temperature and decrease in dew point depression (Figure 6a). HI also shows a sharp decrease prior to the storm which represents the decrease in dew point depression as relative humidity increases (Figure 6b). Sharp increase in PW is seen about 5 h prior to the storm (Figure 6c). This raise corresponds to increase in moisture in the vertical column of the atmosphere. The relative humidity parameter, MEANRH$_{950-850hPa}$ (Figure 6d), shows a sharp increase 4–5 h

earlier to the genesis of thunderstorm, due to increase in the moisture content of the atmosphere. As the storm develops, the sudden increase in moisture along with the storm movement plays a major role in increase of all these instability indices as they are dependent on temperature and moisture contents.

[21] In Figures 7a and 7b, the stability index at two different levels is shown. At the levels 950 and 500 hPa, a the difference in θ_{es} and θ_e is large about 5–6 h in advance, which explains unsaturated atmosphere and as the storm approaches the difference decreases sharply, which corresponds to cool and moist atmosphere [Betts, 1974]. So the decrease in difference of θ_{es} and θ_e at surface 6 h before the storm genesis explains changes in the atmosphere from unsaturated state to saturation which can act as a precursor for the thunderstorm genesis.

[22] The distribution of θ_e LR at different levels in the atmosphere is shown in Figures 8g and 8h. It is clear that 5–6 h prior to the storm, θ_e decreases with height which is a precursor for storm initiation. The parameter θ_e LR$_{950-700hPa}$, showed more negative values prior to the storm which explains more unstable atmosphere. In the lowest layer, θ_e LR sharply increases while it decreases in the middle troposphere prior to the storm due to vertical variation of moisture content (Figures 7c and 7d).

[23] The time series plots of the eight parameters discussed above shows appreciable variations prior to the storm occurrence. From the analysis it is observed that there is an increase in KI by an order of 4°C about 2 h before the storm and relative decrease in HI by 4°–6°C, increase in PW by 0.2–0.4 cm, increase in MEANRH$_{950-850hPa}$ by 20% 5–6 h prior to the storm activity and appreciable variations in stability index and θ_e LR at different levels. The present analysis suggests that using the continuous MWR observations, it may be possible to produce skillful now casts of thunderstorm activity, at least 2–6 h in advance. In the next section,
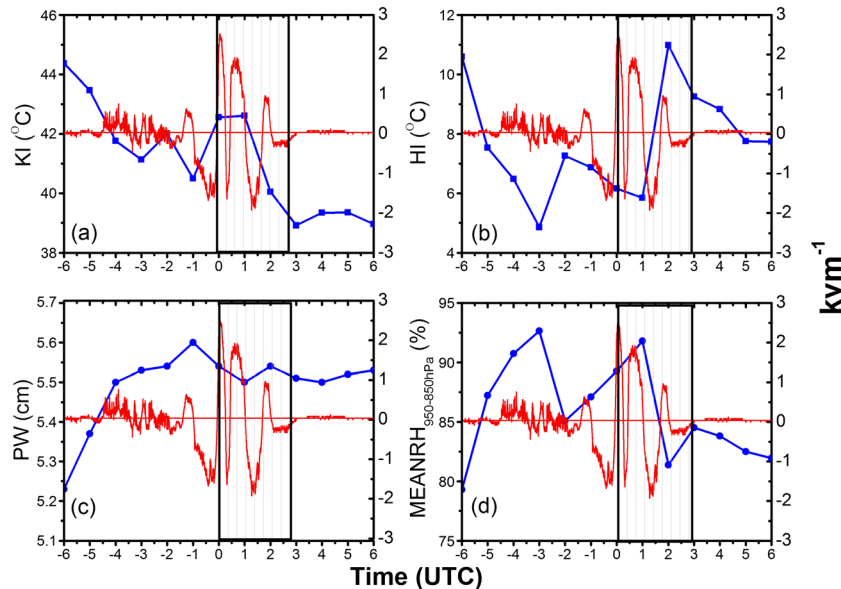
Figure 6. Time series plots of (a) KI, (b) HI, (c) PW, and (d) MEANRH$_{950-850hPa}$ for the thunderstorm case of 27 July 2011 observed using MWR. The electric field strength (red line) observed during same time is also superimposed in all the panels with axis on the right side. The time window represents thunderstorm episode.
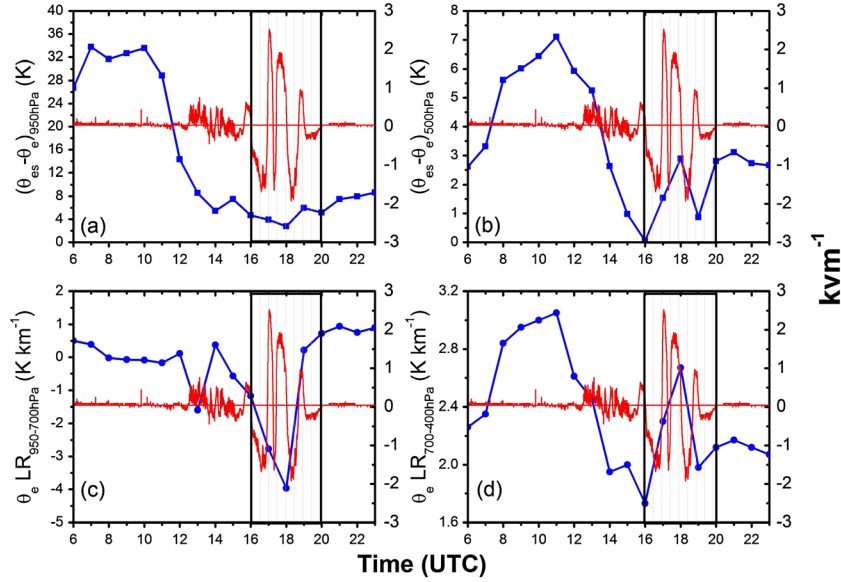
Figure 7. Same as Figure 6, but for (a) the stability index at 950 hPa, (b) the stability index at 500 hPa, (c) θ_e $LR_{950-700\ hPa}$, and (d) θ_e $LR_{700-400\ hPa}$.
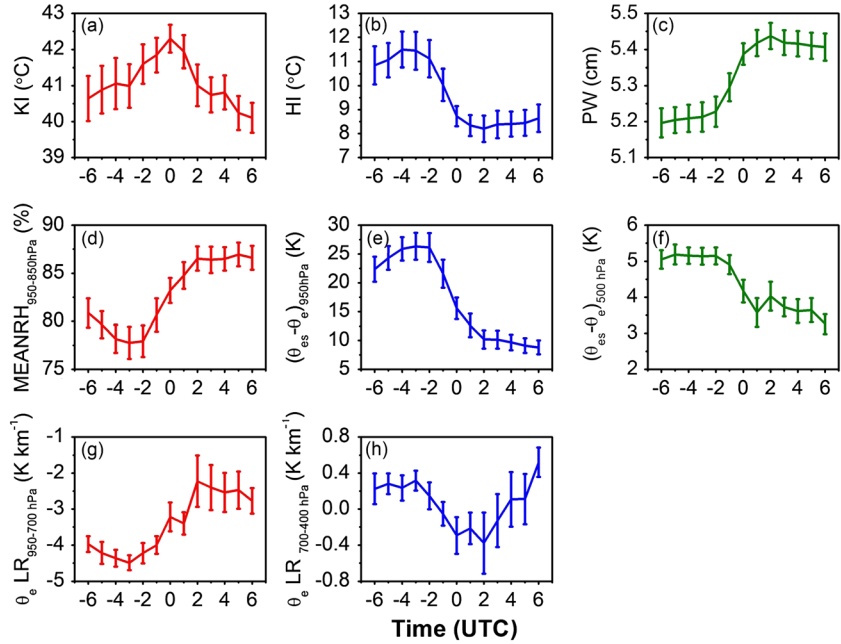
Figure 8. Superepoch analysis of eight different thermodynamical indices. Vertical bars represent the standard errors.

a detailed analysis of variation of thermal indices associated with more number of thunderstorm cases is discussed using a superepoch analysis.

4. Superepoch Analysis

[24] From the analysis discussed above, it inferred that 2–6 h before the storm occurrence, variations in KI, HI, PW, MEANRH$_{950-850hPa}$, stability index and θ_e LR at different levels are clearly observed. These variations in these parameters explain the thermodynamic evolution of the boundary layer convective instability. For obtaining a composite picture

of all thunderstorms considered for the study, we have carried out a superepoch analysis for the time series of various thermal indices derived from MWR observations.

[25] To examine the temporal variations of various thermal indices, lagged composites of all the eight parameters are calculated. The time of occurrence of the storm is considered as lag 0 and lag -6 corresponds to preenvironment 6 h before the storm occurrence and lag +6 correspond to postenvironment 6 h after the storm occurrence. In the present analysis, the hour corresponding to the storm occurrence is considered as zero. Six hours before and after the storm occurrence were superposed and averaged to produce one

superposed curve. This procedure is repeated for all the eight parameters considered in this study. All these parameters corresponding to different lags are averaged and standard deviations are calculated. By observing the variations of the composite time series of these thermodynamic indices, it is possible to explain the prerequisites necessary for the genesis of thunderstorm activity. In the recent study by [*Rajeevan et al.*, 2012], a prediction scheme is developed to nowcast the probability of lightning over southeast India using various thermodynamical indices which explain the tropospheric instability. From the study it is inferred that the above mentioned eight parameters showed appreciable differences in threshold for the occurrence of thunderstorm and nonthunderstorm cases, 60% or more storms are formed when KI exceeds 42°C, MEANRH$_{950-850hPa}$ raises more than 75%, and PW value reaches more than 5.4 cm. And also appreciable variations are observed for stability index and equivalent potential temperature lapse rate at lower and middle levels for thunderstorm and nonthunderstorm cases for the study region. So it is clear that these parameters are historically suitable for this location in nowcasting the genesis of thunderstorm activity in advance. The lag composites of the mentioned eight parameters for the identified 26 thunderstorm cases are shown in Figure 8. KI shows a near monotonic increase from 6 to 0 h prior to the storm. This is due to an increase in vertical lapse rate and low-level moisture and a decrease in dew point depression at 700 mbar. At the time of occurrence of storm, KI exceeding 42°C is observed (Figure 8a). Decrease in HI is also clearly seen before 3 h of the storm occurrence which clearly explains decrease in dew point depression at different levels which suggests increase in relative humidity. HI values are reduced by values less than 10°C (Figure 8b). There is also a sharp increase in total Precipitable water content (PW) and lower-level relative humidity. PW

increases to 5.2 cm or more while lower-level relative humidity (MEANRH$_{950-850hPa}$) exceeds 85% during the storm (Figures 8c and 8d).

[26] $(\theta_{es}-\theta_e)_{950hPa}$ shows a relative decrease 3 h prior to the storm development and decreased by an order of 15 K at the time of storm and the parameter $(\theta_{es}-\theta_e)_{500hPa}$ decreases 2 h before storm genesis and decrease by the order of 2 K as storm approaches. The decrease in these stability index parameters at surface and mid troposphere explains that the parcel is tending to saturation state from unsaturation state of the atmosphere due to increase in relative humidity (Figures 8e and 8f).

[27] θ_e LR$_{950-700hPa}$ increases 3 h prior to the storm occurrence and θ_e LR$_{700-400hPa}$ decreases 3 h before the storm initiation. θ_e LR at both levels is negative which corresponds to unstable atmosphere but at lower levels increase is seen prior to the storm whereas at middle levels decrease is seen this is due to variation on water vapor density at different levels. Since the vertical distribution of θ_e depends on the amount of water vapor the increase in moisture at lower levels during the initiations of storm results in increasing of θ_e LR$_{950-700hPa}$ as compared to the other (shown in Figures 8g and 8h).

[28] However, the observed variations associated with thunderstorms could happen during nonthunderstorm cases also due to diurnal variation of temperature, moisture and boundary layer. Therefore, to examine the kind of variations to be observed during nonthunderstorm cases, we considered 30 nonthunderstorm cases, selected randomly. Since superposed epoch analysis (with zero time) cannot be applied for the nonthunderstorm cases, composites (arithmetic averages) of the parameters during the period 0600–1800 UTC were calculated and examined. Majority (90% or more) of storm occurrence at Gadanki is observed during the period 0600–1800 UTC. The average variations of the
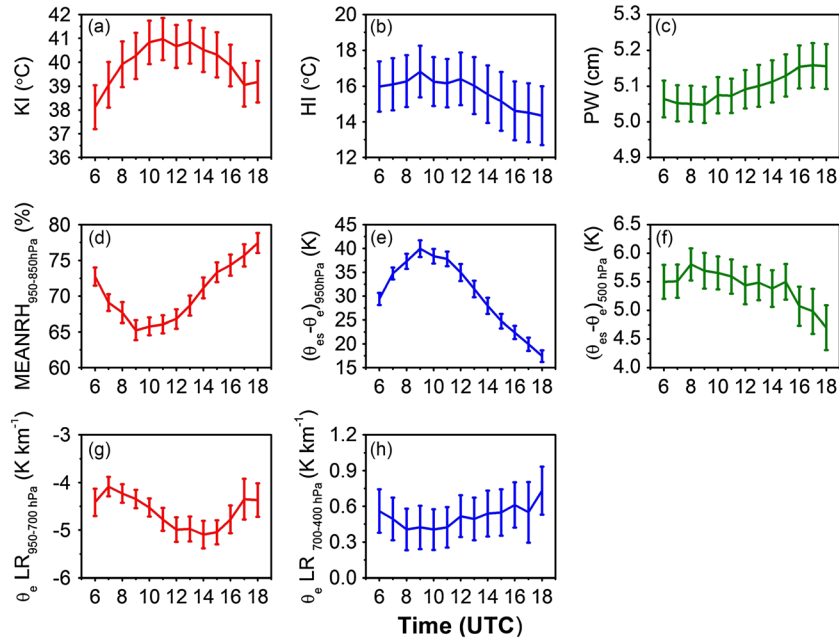
Figure 9. Composite profiles of eight different thermodynamical parameters along with standard errors (vertical lines) for nonthunderstorm cases.

eight parameters for nonthunderstorm cases are shown in Figures 9a–9h.

[29] For nonthunderstorm cases also KI shows an increase in value during the evening, but however the mean value of KI (less than 40) for nonthunderstorm days is much less than KI (more than 42) observed during the thunderstorm days and moreover for thunderstorm cases, KI shows a monotonic increase as storm approaches which is not seen for nonthunderstorm cases. HI does not show sharp decrease as observed during the thunderstorm cases. Moreover, the value of HI for nonthunderstorm cases is also larger compared to thunderstorm cases. Similarly, PW during nonthunderstorm days does not show a sharp increase and the mean value of PW during nonthunderstorm cases is less than thunderstorm cases. Even though $MEANRH_{950-850hPa}$ shows an increase during the evening period, the mean value of this parameter (less than 70%) for nonthunderstorm days is much less than the mean value (more than 80%) during the thunderstorm cases. Similarly, $(\theta_{es}-\theta_e)_{950hPa}$ shows a sharper decrease during the thunderstorm days compared to nonthunderstorm days. The magnitude of this parameter during the nonthunderstorm days is much larger than during thunderstorm cases. The same parameter at 500 hPa also shows a sharp decrease during the thunderstorm cases. The parameters θ_e $LR_{950-700\ hPa}$, θ_e $LR_{700-400\ hPa}$ do not show appreciable variations during the nonthunderstorm cases as observed in thunderstorm cases (shown in Figures 9a–9h).

[30] Thus we note appreciable differences in the variations and magnitude of the parameters between thunderstorm and nonthunderstorm cases. This information may be useful for developing an algorithm for nowcasting purposes. In the next section, we discuss the possibility of nowcasting thunderstorms (at least 2 h in advance) using these eight parameters derived from MWR data.

5. Independent Cases

[31] Superepoch analysis has been done to obtain the composite picture of variations of MWR derived indices with the occurrence of intense convective activity. The information so established could be useful for nowcasting of intense convective weather. For testing the information revealed from superepoch analysis to nowcast thunderstorm activity, we have done an independent verification using nine thunderstorm cases. The nine thunderstorm cases identified for the analysis is shown in Table 2. These cases were not included in the superposed epoch analysis discussed in section 4. The superposed epoch variations of the mean of parameters

Table 2. List of Thunderstorm Cases

Storm	Thunderstorm Date
1	1 Jul 2011
2	5 Jul 2011
3	9 Oct 2011
4	7 Jun 2012
5	10 Jul 2012
6	17 Jul 2012
7	21 Aug 2012
8	29 Aug 2012
9	3 Sep 2012

during the nine cases of thunderstorms are shown in Figures 10a–10h along with the superposed epoch variations of 26 thunderstorms considered in the earlier analysis. The results indicate similar kind of variations during these nine cases of thunderstorms also except for a couple of parameters.

[32] The parameter KI during the nine cases is showing an increasing trend before the storm occurrence as we observed in the superepoch analysis. Mean value of KI is larger than the superepoch analysis of 26 cases. HI shows a sharp decrease and PW shows a sharp increase. Similarly, mean RH in the lower level ($MEANRH_{950-850hPa}$) increases sharply. And θ_e differences parameters ($\theta_{es}-\theta_e)_{950hPa}$ and $(\theta_{es}-\theta_e)_{500hPa}$ also shows sharp decreases as we have seen in the superepoch analysis of 26 thunderstorm cases. Both θ_e lapse rate parameters θ_e $LR_{950-700\ hPa}$, θ_e $LR_{700-400\ hPa}$ also show similar variations as observed in the superepoch analysis.

[33] The above results during the independent period suggest the importance of examining the temporal variation of various thermal and moisture parameters in nowcasting thunderstorm activity. It clearly highlights the importance of continuous monitoring of thermal indices from MWR to nowcast the severe thunderstorm activity in advance.

6. Conclusions

[34] The primary objective of the present paper is to demonstrate the use of ground-based microwave radiometer for studying severe convective activity over Southeast Indian region and exploring the feasibility of nowcasting thunderstorm activity at least 2 h in advance. For this purpose, continuous observations of temperature and moisture obtained from MWR located at a tropical station, Gadanki were used. Before using MWR data for the analysis of thunderstorm cases, the quality of MWR data is validated by comparing the temperature and vapor density profiles with that observed from colocated GPS radiosonde data. The analysis revealed that the MWR derived profiles of temperature and vapor density match reasonably well with the GPS radiosonde profiles. Moreover, at least 15 thermodynamic variables derived from MWR data correlated significantly (statistically significant) with the variables derived from GPS radiosonde observations.

[35] To examine the utility of the continuous measurements by MWR, we have carried out a superepoch analysis of eight thermodynamic parameters derived from MWR data for 26 thunderstorm cases. The superepoch analysis is conducted from 6 h before the storm initiation to 6 h after the storm initiation. This analysis suggested that many thermodynamic parameters like, KI, LI, total precipitable water content, lower-level relative humidity, stability index at different levels, lapse rate of equivalent potential temperature showed useful signals at least 3 h before the storm occurrence. The analysis showed that there are sharp changes in the eight thermodynamic parameters associated with the storms. There are appreciable differences in the variations of these eight parameters between thunderstorm and nonthunderstorm cases.

[36] The present study thus highlights the utility of ground-based MWR observations for studying and nowcasting thunderstorms. However, the present study has some caveats, especially on the nowcasting method. The present study uses only limited cases of thunderstorms. The
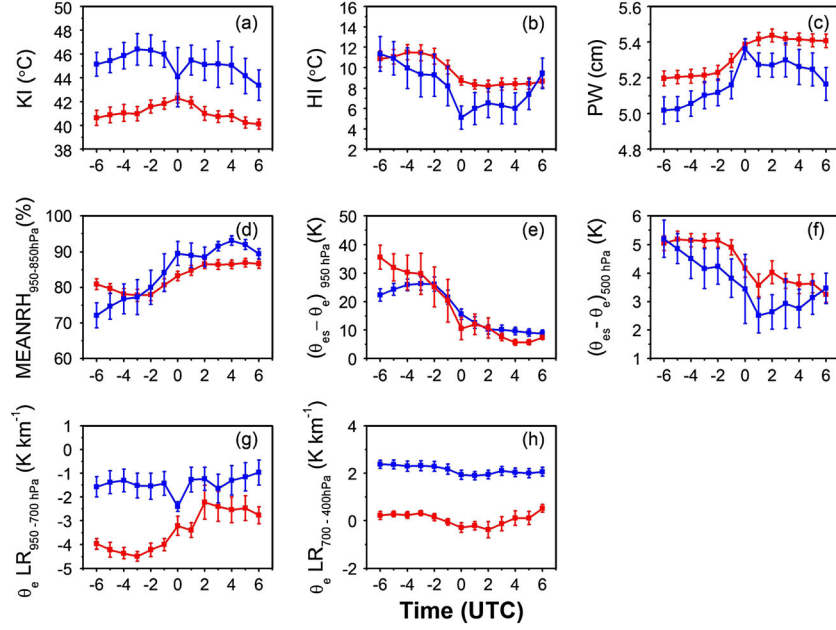
Figure 10. Composite profiles of mean of nine thunderstorm cases along with standard deviations (blue line) considered for independent verification along with superposed epoch analysis (red line) of eight instability parameters.

robustness of the present results will improve with more number of thunderstorm cases. Similarly, some quantitative expert/statistical systems also need to be developed for nowcasting thunderstorm occurrence using the ground-based MWR observations. Even though objective criterion was established for each parameter considered in the study, development of a quantitative method for nowcasting thunderstorm activity is required which will form our future study.

Appendix A

[37] Many indices for quantitatively estimating tropospheric static stability have been applied in weather forecasting. Most indices combine measures of the thermal and moisture properties of low to middle troposphere. Many of them were developed to aid in the forecasting of thunderstorms or severe weather [e.g., *Galway*, 1956; *George*, 1960; *Miller*, 1967; *Peppler and Lamb*, 1989].

[38] In the present study, various thermodynamic stability indices are computed by using temperature, relative humidity profiles. They are classified into eight basic categories; all these indices explain thermodynamic structure of atmosphere from surface to upper troposphere by explaining moisture, instability of atmosphere which is necessary for storm to initiate.

1. The first category is single-level indices, such as LI, KI, TTI, and HI:

$$LI = T_{p500} - T_{500}$$

$$KI = (T_{850} - T_{500}) + T_{d850} - (T_{700} - T_{d700})$$

$$TT = T_{850} + T_{d850} - 2T_{500}$$

$$HI = (T - Td)_{850} + (T - Td)_{700} + (T - Td)_{500}$$

where T_p is parcel Temperature, T is air temperature, Td is dew point temperature.

2. The second category is integrated indices, such as LCAPE2 [*Rajeevan et al.*, 2012] and CINE.
3. The third category is moisture parameters, such as precipitable water content (PW) [*Solot*, 1938] and various relative humidity (RH) parameters, such as mean relative humidity from 950 to 850 hPa (MEANRH$_{950-850hPa}$), relative humidity at freezing level (RHFRZL), and mean layer relative humidity (MEANLAYRH) of the whole atmospheric column.
4. Layer thicknesses between the different layers of atmosphere are denoted by THICKNESS$_{950-850hPa}$, THICKNESS$_{850-500hPa}$, THICKNESS$_{700-400hPa}$, and THICKNESS$_{500-300hPa}$.
5. The stability index at different levels, $(\theta_{es}-\theta_e)_{950hPa}$, $(\theta_{es}-\theta_e)_{850hPa}$, $(\theta_{es}-\theta_e)_{500hPa}$, is also considered. It is obtained by calculating the difference between θ_{es} and θ_e. It explains the state of atmosphere.
6. Temperature lapse rate (LR) at different levels, LR$_{950-700hPa}$, LR$_{700-400hPa}$, and LR$_{400-300hPa}$, and θ_e lapse rate (θ_e LR) at different levels, θ_e LR $_{950-700\ hPa}$, θ_e LR$_{700-400\ hPa}$, and θ_e LR$_{400-300\ hPa}$, explain instability present in the atmosphere.
7. Convective temperature (CONVTEMP) explains the surface heating results in rising of parcel without any mechanical lift.
8. The shape factor (SF) explains the vertical gradient of equivalent potential temperature θ_e to examine the severity of atmospheric instability.

References

Beebe, R. G. (1958), Tornado proximity soundings, *Bull. Am. Meteorol. Soc.*, *39*, 195–201.

Betts, K. A. (1974), Thermodynamic classification of tropical convective soundings, *Mon. Weather Rev.*, *102*, 760–764.

Bluestien, H. B., and S. Parker (1993), Modes of isolated convective storm formation along the dryline, *Mon. Weather Rev.*, *121*, 1354–1372.

Brooks, H. E., C. A. Doswell III, and R. B. Wilhelmson (1994), The role of midtropospheric winds in the evolution and maintenance of low-level mesocyclones, *Mon. Weather Rev.*, *122*, 126–136.

Browning, K. A. (1980), Local weather forecasting, *Proc. R. Soc. London, Ser. A.*, *371*, 179–211.

Cady-Pereria, E. K., M. W. Shephard, D. D. Turner, E. J. Mlawer, S. A. Clough, and T. J. Wagner (2008), Improved daytime column-integrated precipitable water vapor from Vaisala radiosonde humidity sensors, *J. Atmos. Oceanic Technol.*, *25*, 873–883.

Carlson, S., G. Benjamin, G. S. Forbes, and Y. F. Li (1983), Elevated mixed layer in the severe-storm environment conceptual model and case studies, *Mon. Weather Rev.*, *111*, 1453–1473.

Chan, P. W. (2009), Performance and application of a multi-wavelength, ground based microwave radiometer in intense convective weather, *Meteorol. Z.*, *18*(3), 253–265.

Chan, P. W., and K. K. Hon (2011), Application of ground-based, multi-channel microwave radiometer in the nowcasting of intense convective weather through instability indices of the atmosphere, *Meteorol. Z.*, *20* (4), 431–440.

Chan, P. W., and Y. F. Lee (2011), Application of a ground-based, multi-channel microwave radiometer to the alerting of low-level windshear at an airport, *Meteorol. Z.*, *20*(4), 423–429.

Clifford, S. F., J. C. Kaimal, R. J. Lataitis, and R. G. Strauch (1994), Ground-based remote profiling in atmospheric studies, An overview, *Proc. IEEE*, *82*, 313–355.

Colby, F. P. (1984), Convective inhibition as a predictor of convection during AVE-SESAME II, *Mon. Weather Rev.*, *112*, 2239–2252.

Dupilka, M. L., and G. W. Reuter (2005), Forecasting tornadic thunder-storm potential in Alberta using environmental sounding data. Part II: Helicity, precipitable water, and storm convergence, *Weather Forecast.*, *21*, 336–346.

Feltz, W. F., and J. R. Mecikalski (2002), Monitoring high-temporal-resolution convective stability indices using the ground-based Atmospheric Emitted Radiance Interferometer (AERI) during the 3 May 1999 Oklahoma–Kansas tornado outbreak, *Weather Forecast.*, *17*, 445–455.

Feltz, W. F., W. L. Smith, H. B. Howell, R. O. Knuteson, H. Woolf, and H. Revercomb (2003), Near-continuous profiling of temperature, moisture, and atmospheric stability using the Atmospheric Emitted Radiance Inter-ferometer (AERI), *J. Appl. Meteorol.*, *42*, 584–597.

Galway, J. G. (1956), The lifted index as a predictor of latent instability, *Bull. Amer. Meteor. Soc.*, *37*, 528–529.

Geerts, B. (2001), Estimating downburst-related maximum surface wind speeds by means of proximity soundings in New South Wales, Australia, *Weather Forecast.*, *16*, 261–269.

George, J. J. (1960), *Weather Forecasting for Aeronautics*, pp. 407–415, Academic Press, New York.

Güldner, J., and D. Spänkuch (1999), Results of year-round remotely sensed integrated water vapor by ground-based microwave radiometry, *J. Appl. Meteorol.*, *38*, 981–988.

Güldner, J., and D. Spänkuch (2001), Remote sensing of the thermody-namic state of the atmospheric boundary layer by ground-based micro-wave radiometry, *J. Atmos. Oceanic Technol.*, *18*, 925–933.

Haklander, A., and A. J. van Delden (2003), Thunderstorm predictors and their forecast skill for the Netherlands, *Atmos. Res.*, *67–68*, 273–299.

Hering, A. M., C. Morel, G. Galli, S. Sénési, P. Ambrosetti, and M. Boscacci (2004), Nowcasting thunderstorms in the alpine region using radar based adaptive thresholding scheme, paper presented at 3rd European Conf. Radar in Meteorology and Hydrology (ERAD), Visby, Sweden, 6–10 Sept. [Available at http://www.copernicus.org/erad/2004/online/ERAD04_P_206.pdf.]

Jacovides, C. P., and T. Yonetani (1990), An evaluation of stability indi-ces for thunderstorm prediction in greater Cyprus, *Weather Forecast.*, *5*, 559–569.

Khalsa, S. J. S. (1989), Atmospheric stability over the tropical oceans derived from TIROS operational vertical sounder, *J. Appl. Meteorol.*, *28*, 1002–1009.

Kober, K., and A. Tafferner (2009), Tracking and nowcasting of convective cells using remote sensing data from radar and satellite, *Meteorol. Z.*, *1*, 75–84.

Koffi, E. (2007), The use of radiometer derived convective indices in thunderstorm nowcasting, *Res. Rep. 2007-02-MW*, 31 pp., Inst. of Appl. Phys., Univ. of Bern, Bern.

Knupp, K., R. Ware, D. Cimni, F. Vandenberghe, J. Vivekanandan, E. Westwater, and T. Coleman (2009), Ground-based passive microwave profiling during dynamic weather conditions, *J. Atmos. Oceanic Technol.*, *26*, 1057–1072.

Lambert, W. C., M. Wheeler, and W. Roeder (2005), Objective lightning forecasting at Kennedy Space Center and Cape Canaveral Air Force Station using cloud-to-ground lightning surveillance system data, paper presented at Conference on Meteorological Applications of Lightning Data, Am. Meteorol. Soc., San Diego, Calif.

Lee, O. S. M. (2007), Forecast of strong gusts associated with thunder-storms based on data from radiosonde ascents and automatic weather stations [in Chinese], paper presented at 21st Guangdong–Hong Kong–Macao Technical Seminar on Meteorological Science and Technology, Hong Kong, 24–26 Jan.

Litynska, Z., J. Parfiniewicz, and H. Pinkowski (1976), The prediction of air mass thunderstorms and hails, *W. M. O. Bull.*, *450*, 128–130.

Manzato, A. (2003), A climatology of instability indices derived from Friuli Venezia Giulia soundings, using three different methods, *Atmos. Res.*, *67–68*, 417–454.

Marinaki, A., M. Spliiotopolous, and H. Michalopoulou (2006), Evaluation of atmospheric instability indices in Greece, *Adv. Geosci.*, *7*, 131–135.

McCann, D. W. (1994), WINDEX—A new index for forecasting micro-burst potential, *Weather Forecast.*, *9*, 532–541.

Miller, R. C. (1967), Notes on analysis and severe storm forecasting proce-dures of the Military Weather Warning Center. Tech. Report 200, AWS, USAF. [Headquarters, AWS, Scott AFB, 1L 62225].

Murphy, M. J., R. L. Holle, and N. W. S. Demetriades (2008), Cloud-to-ground lightning warnings using electric field mill and lightning observa-tions, paper presented at the 19th International Lightning Detection Conference, Vaisala, Inc., Tucson, Ariz.

Nath, D., M. Venkat Ratnam, V. V. M. Jagannadha Rao, B. V. Krishna Murthy, and S. Vijaya Bhaskara Rao (2009), Gravity wave characteris-tics observed over a tropical station using high-resolution GPS radio-sonde soundings, *J. Geophys. Res.*, *114*, D06117, doi:10.1029/2008JD011056.

Peppler, R. A., and P. J. Lamb (1989), Tropospheric static stability and cen-tral north American growing season rainfall, *Mon. Weather. Rev.*, *117*, 1156–1180.

Rajeevan, M., A. Kesarkar, S. B. Thampi, T. N. Rao, B. Radhakrishna, and M. Rajasekhar, (2010), Sensitivity of WRF cloud microphysics to simula-tions of a severe thunderstorm event over southeast India, *Ann. Geophys.*, *28*, 603–619.

Rajeevan, M., A. Madhulatha, M. Rajasekhar, J. Bhate, A. Kesarkar and B. V. Apparao (2012), Development of a perfect prognosis probabilistic model for prediction of lightning over south-east India, *J. Earth Syst. Sci.*, *121*, 355–371.

Reap, R. M. (1994), 4–h NGM based probability and categorical forecasts of thunderstorms and severe local storms for the contiguous U.S., *NWS Tech. Proc. Bull. 419*, 14 pp., Natl. Weather Serv., Silver Spring, Md.

Rose, T., and H. Czekala (2003), Filter bank radiometers for atmospheric profiling, paper presented at Sixth International Symposium on Tropo-spheric Profiling: Needs and Technologies. Meckenhiem, Germany.

Sanders, F. (1986), Temperatures of air parcels lifted from the surface: Back-ground, application, and monograms, *Weather Forecast.*, *1*, 190–205.

Sanders, F., and D. O. Blanchard (1993), The origin of a severe thunder-storm in Kansas on 10 May 1985, *Mon. Weather Rev.*, *121*, 133–149.

Shafer, P. E., and H. E. Fuelberg (2006), A statistical procedure to forecast warm season lightning over portions of the Florida peninsula, *Weather Forecast.*, *21*, 851–868.

Solot, B. (1938), Computation of depth of precipitable water in a column of air, *Mon. Weather Rev.*, *67*, 100–103.

Tuduri, I. E., and C. Ramis (1997), The environments of significant convective events in the western Mediterranean, *Weather Forecast.*, *12*, 294–306.

Walker, I., V. Chakrapani, and W. El Mahboub (2008), The development of a shape factor instability index to guide severe weather forecasts for aviation safety, *Meteorol. Appl.*, *15*, 465–473.

Ware, R., R. Carpenter, J. Guldner, J. Liljegren, T. Nehrkorn, F. Solheim, and F. Vandenberghe (2003), A multichannel radiometric profiler of

temperature, humidity, and cloud liquid, *Radio Sci.*, *44*(3), 8079, doi:10.1029/2002RS002856.

Westwater, E. R., B. Stankov, D. Cimini, Y. Han, J. A. Shaw, B. M. Lesht, and C. N. Long (2003), Radiosonde humidity soundings and microwave radiometers during Nauru99, *J. Atmos. Oceanic Technol.*, *20*(7), 953–971.

Wilczak, J. M., E. E. Gossard, W. D. Neff, and W. L. Eebrehard (1996), Ground based remote sensing of the atmospheric boundary layer: 25 years of progress, *Boundary Layer Meteorol.*, *71*, 277–296.

Wilson, J. W., and C. K. Mueller (1993), Nowcasts of thunderstorm initialization and evolution, *Weather Forecast.*, *8*, 113–131.

Wilson, J. W., N. A. Crook, C. K. Mueller, J. Sun, and M. Dixon (1998), Nowcasting thunderstorms: A status report, *Bull. Am. Meteorol. Soc.*, *79*, 2079–2099.

Won, H. Y. (2009), An application of brightness temperature received from a ground-based microwave radiometer to estimation of precipitation occurrences and rainfall intensity, *J. Atmos. Sci.*, *45*, 55–69.